Dissecting the Molecular Structure of the Air/Ice Interface from Quantum Simulations of the Sum-Frequency Generation Spectrum

Richa Rashmi*,† and Francesco Paesani*,†,‡,¶,§

†*Department of Chemistry and Biochemistry, University of California San Diego, La Jolla, California 92093, United States*

‡*Materials Science and Engineering, University of California San Diego, La Jolla, California 92093, United States*

¶*Halicioğlu Data Science Institute, University of California San Diego, La Jolla, California 92093, United States*

§*San Diego Supercomputer Center, University of California San Diego, La Jolla, California 92093, United States*

E-mail: rrashmi@ucsd.edu; fpaesani@ucsd.edu

Abstract

Ice interfaces are pivotal in mediating key chemical and physical processes, such as heterogeneous chemical reactions in the environment, ice nucleation, and cloud microphysics. At the ice surface, water molecules form a quasi-liquid layer (QLL) with distinct properties from the bulk. Despite numerous experimental and theoretical studies, the molecular-level understanding of the QLL has remained elusive. In this work, we use state-of-the-art quantum dynamics simulations with a realistic data-driven many-body potential to dissect the vibrational sum-frequency generation (vSFG) spectrum of

the air/ice interface in terms of contributions arising from individual molecular layers, orientations, and hydrogen-bonding topologies that determine the QLL properties. The agreement between experimental and simulated spectra provides a realistic molecular picture of the evolution of the QLL as a function of temperature without the need for empirical adjustments. The emergence of specific features in the experimental vSFG spectrum suggests that surface restructuring may occur at lower temperatures. This work not only underscores the critical role of many-body interactions and nuclear quantum effects in understanding ice surfaces but also provides a definitive molecular-level picture of the QLL, which plays a central role in multiphase and heterogeneous processes of relevance to a range of fields, including atmospheric chemistry, cryopreservation, and materials science.

Introduction

The abrupt truncation of the water hydrogen-bond network at the air/ice interface forces water molecules to adopt configurations significantly different from those in bulk ice.[1] This leads to dangling OH bonds with greater mobility and reactivity, causing disorder within the top layers of ice and forming a quasi-liquid layer (QLL) below the freezing point of water (premelting).[2] The molecular structure of the QLL mediates several fundamental phenomena, including phase transitions,[3] ice crystallization,[4,5] and chemical reactions occurring on ice surfaces.[6,7]

First reported by Michael Faraday in the 1850s, the QLL was initially proposed to explain the phenomenon of regelation.[8] However, it took another century before experimental techniques were developed that could quantitatively probe the ice surface structure.[9] These techniques needed to be surface-specific and minimally invasive, as the ice surface is very thin and can easily melt or deform irreversibly. Advanced optical microscopy techniques, such as laser confocal microscopy combined with differential interference contrast microscopy (LCM-DIM), have suggested that the QLL can exhibit a range of wetting morphologies, from

complete wetting (liquid-layer type) to partial wetting (droplet-type) states, depending on the interfacial free energies.[10–12] Other experimental methods, such as ellipsometry,[13] X-ray diffraction,[14] X-ray absorption,[15] atomic force microscopy (AFM),[16] and scanning tunneling microscopy (STM),[17] have predicted the premelting temperature to be between 200 K and 260 K, with QLL thicknesses ranging from 1 nm to 100 nm. This discrepancy is generally attributed to differences in sample purity and the varying surface sensitivity of the experimental techniques.[18] Recent AFM studies have shown that the ice surface may consist of mixed hexagonal ice (I_h) and cubic ice (I_c) structures due to stacking disorder.[19]

Vibrational sum-frequency generation (vSFG) spectroscopy is an ideal technique for probing the properties of ice interfaces, as it does not require a high-vacuum environment and is intrinsically interface-selective.[20] By adjusting the light polarization, vibrational modes corresponding to different orientations of water molecules at the air/ice interface can be selectively enhanced, allowing for the study of lateral and longitudinal interactions. Within the dipole approximation, a vSFG spectrum depends only on the second-order nonlinear susceptibility, $\chi^{(2)}$, which is zero in bulk (centrosymmetric) media but non-zero at the interface. Since the second-order susceptibility can be resolved into real and imaginary components, both real and imaginary components of a vSFG spectrum can be measured. The imaginary spectrum is particularly useful for understanding molecular orientations, as positive and negative spectral features correspond to molecular dipole moments pointing toward and away from the surface, respectively.

The first experimental vSFG spectra of the air/ice interface – where ice hereafter refers to ice I_h unless otherwise specified – measured by Shen and coworkers,[21,22] revealed a relatively narrow band around 3700 cm^{-1}, corresponding to the stretching motion of free OH groups, and a broad band centered at ∼3150 cm^{-1}, attributed to the stretching motion of hydrogen-bonded OH groups. Subsequent measurements down to 113 K showed that the vSFG spectra of the prismatic and basal planes of ice I_h are similar and attributed the spectral feature at 3100 cm^{-1} to bilayer stitching hydrogen bonds, with a significant quadrupole

contribution noted.[23–25] In these spectra, the intensity of the hydrogen-bonded region was found to increase significantly with decreasing temperature, although both peak positions and intensities differed from those initially reported in Refs. 21 and 22. With the development of heterodyne-detected vSFG (HD-vSFG) spectroscopy, the first spectra of the air/ice interface directly reporting the imaginary component of the nonlinear susceptibility were independently measured by the Bakker and Yamaguchi groups in 2017.[26–28] Although both sets of spectra from these independent measurements display a positive feature around 3100 cm^{-1}, they differ significantly at higher frequencies. More recent vSFG measurements have indicated that crystalline ice undergoes bilayer-by-bilayer surface melting to form a QLL at the air/ice interface, with the first bilayer melting at 200 K and the second at 257 K.[29] It has also been suggested that the vibrational properties of the QLL are similar to those of supercooled water.[26]

On the theoretical side, Buch and coworkers first calculated the vSFG spectrum of the air/ice interface in 2007 using an exciton model for the OH-stretch vibrations.[30] While the model captured the main features of the experimental spectrum, it failed to reproduce all spectral details, primarily due to the neglect of vibrational coupling. Subsequent theoretical vSFG calculations suggested that the ice surface exhibits a proton ordering pattern, known as the Fletcher pattern, rather than random proton ordering.[31] Quantum mechanics/molecular mechanics (QM/MM) simulations combined with the charge response kernel (CRK) model were also used to calculate the HD-vSFG spectrum of the air/ice interface, successfully reproducing the intense negative band in the hydrogen-bonded region, as well as the small positive feature at 3100 cm^{-1}.[32] However, these simulations predicted the spectral features at higher frequencies than those observed experimentally, requiring an artificial red-shift of the theoretical spectrum. The HD-vSFG spectrum of the air/ice interface in the OH-stretch frequency region has also been calculated using *ab initio* molecular dynamics (AIMD) simulations based on density functional theory (DFT).[33] In this case as well, the theoretical spectrum required an artificial red-shift to align with the experimental measure-

ments. Overall, all previous theoretical studies underscore that a realistic description of the air/ice interface depends critically on an accurate representation of molecular interactions and a proper account of nuclear quantum effects (NQEs).

Contradictory experimental results and inadequate theoretical models have thus far prevented a comprehensive understanding of the molecular properties of the ice surface and the associated QLL. To overcome this challenge, we employ DNN@MB-pol,[34–36] a deep neural network potential trained on the highly accurate MB-pol potential energy function,[37,38] to simulate the air/ice interface as a function of temperature below the melting point. Molecular trajectories generated with DNN@MB-pol are then used to calculate the corresponding HD-vSFG spectra through both classical molecular dynamics (MD) simulations and quantum temperature-elevated path integral coarse-graining (Te-PIGS) simulations[39,40] performed with MB-pol(2023), the latest version of the MB-pol potential that exhibits enhanced accuracy.[41] By systematically dissecting the spectral features in terms of distinct hydrogen-bonding topologies, we provide a detailed molecular-level picture of the QLL at the air/ice interface as a function of temperature, accurately accounting for many-body molecular interactions and NQEs, while addressing limitations that have affected previous theoretical studies.

Results and discussion

Structure of the air/ice interface. Ice I_h forms a bilayer structure along the c-axis, which is perpendicular to the basal plane, with the topmost bilayer serving as the air/ice interface. Fig. 1 shows a snapshot of the simulated proton-disordered air/ice slab at $T = 200$ K, including two equivalent interfaces, the oxygen density profile along the c-axis, and the definition of the molecular monolayers (ML) and bilayers (BL). Additional structural details are reported in Fig. S3 and S4 of the Supporting Information, which illustrate the disorder induced by surface premelting. This disorder was determined by monitoring the variation in

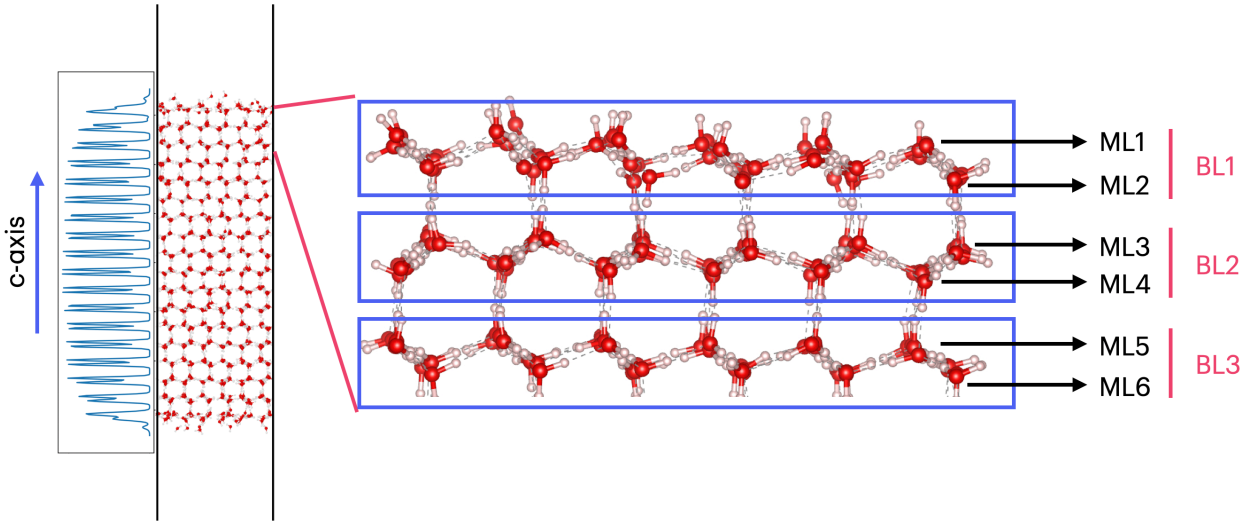

Figure 1: Snapshot of the simulated air/ice interface slab, including two interfaces, the oxygen density profile along the c-axis, and the definition of the molecular monolayers (ML) and bilayers (BL).

the number of melted bilayers along classical MD trajectories performed with the DNN@MB-pol potential at temperatures $T - T_{\mathrm{m}} = -62$ K, -12 K, and -2 K, where $T_m = 262.5$ K is the melting point of ice predicted by the DNN@MB-pol potential.[34] Using the environment similarity kernel (see Fig. S2 of the Supporting Information),[42] we determined that, on average, approximately 1, 1.5, and 4 bilayers are melted at $T - T_{\mathrm{m}} = -62$ K, -12 K, and -2 K, respectively. Notably, the ice surface at $T - T_{\mathrm{m}} = -2$ K exhibits a larger variation in the number of melted water molecules and undergoes a bilayer-by-bilayer melting (see Fig. S5 of the Supporting Information) as observed experimentally.[29] To ensure appropriate sampling of initial configurations, 20 configurations representing the full range of melted bilayers in correct proportions were selected from the equilibrated air/ice slab structures (see Sections IV and V of the Supporting Information) for simulating the vSFG spectra.

vSFG spectrum of the air/ice interface. The vSFG spectra of the air/ice interface were simulated for the SSP polarization combination, where S and P denote laser polarizations parallel and perpendicular to the surface, respectively (see Section VI of the Supporting Information for details). For ease of comparison, all vSFG spectra are normalized relative

to the intensity of the free OH peak at T – T_m = -62 K. For simplicity, we refer to the imaginary component of the vSFG spectra simply as "vSFG spectra" throughout the following analyses. Fig. 2 shows the vSFG spectra calculated from classical MD and quantum Te-PIGS simulations with MB-pol(2023), alongside the corresponding experimental spectra at three temperatures (see Sections II and III of the Supporting Information for specific theoretical and computational details). For ease of comparison, a constant red-shift of 190 cm^{-1} is applied to the classical vSFG spectra to approximately account for NQEs, which are neglected in classical MD simulations, and match the experimental free OH peak frequency. No frequency shift is applied to the corresponding quantum Te-PIGS vSFG spectra. Both classical MD and quantum Te-PIGS vSFG spectra of the the air/ice interface predict four distinct spectral features: (i) a pronounced peak at 3700 cm^{-1} originating from dangling OH bonds exposed to air, (ii) a positive peak at 3550 cm^{-1}, (iii) a small positive shoulder at 3450 cm^{-1} that develops into a peak at lower temperatures, and (iv) a broad negative band between 3200 and 3400 cm^{-1}, attributed to the stretching vibrations of hydrogen-bonded OH groups. The vSFG spectra calculated from quantum Te-PIGS simulations closely reproduce the frequencies of all the experimental spectral features, with deviations of $\Delta\omega \leq 50$ cm^{-1}, consistent with previous simulations of vibrational spectra using MB-pol,[43–48] providing fur-

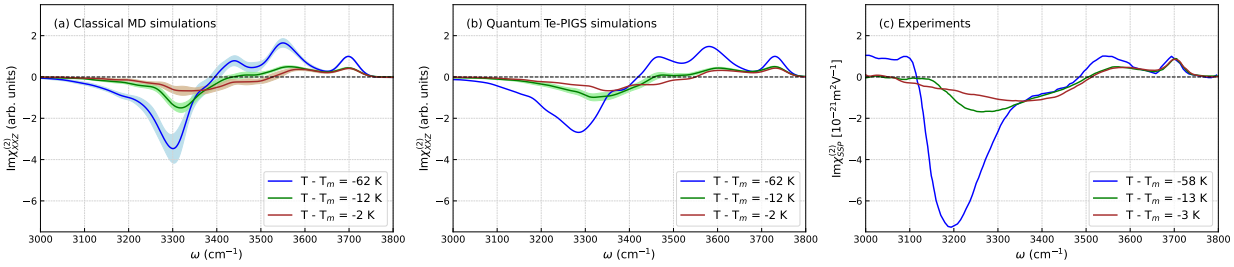

Figure 2: Classical MD and quantum Te-PIGS vSFG spectra of the air/ice interface, calculated at three temperatures with MB-pol(2023), compared with the corresponding experimental spectra.[26,27] For ease of comparison, the classical spectra are red-shifted by 190 cm^{-1} to align with the experimental free OH peak frequency. All vSFG spectra were calculated for the SSP polarization combination. Error bars on the simulated vSFG spectra represent 95% confidence intervals, calculated from the standard error of the mean across 10 and 20 independent trajectories for $T - T_m = -62$ K, and $T - T_m = -12$ K and -2 K, respectively.

ther evidence of the predictive capability of the MB-pol(2023) potential.[41]

The most notable difference between the experimental and simulated vSFG spectra is the absence of a low-frequency positive feature (3000–3100 cm^{-1}) in the latter at lower temperatures. A similar discrepancy was observed in the vSFG spectra of the air/water interface, which was later attributed to phase artifacts in the experimental spectra.[49] In the case of the air/ice interface, the emergence of the low-frequency positive feature at low temperatures may also be due to surface restructuring.[19] It should also be noted that the shoulder at $\sim$3450 cm^{-1} in both classical MD and quantum Te-PIGS vSFG spectra at higher temperatures develops into a distinct peak at $T-T_m = -62$ K, whereas, in the experimental spectra, this feature begins to emerge at $T - T_m \approx -120$ K and is less pronounced. This discrepancy may arise from small differences in the vibrational frequency shifts of non-vertical OH bonds of water molecules within a bilayer whose vertical OH bonds form hydrogen bonds with molecules in the bilayer above or below, resulting in more pronounced positive contributions in the simulated vSFG spectrum (see subsection "Spectra decomposition" below). Moreover, while the simulated vSFG spectra successfully replicate the intensity of the negative hydrogen-bonded band at $T - T_m = -12$ K and $T - T_m = -2$ K, they fall short of capturing its pronounced intensity at $T - T_m = -62$ K. This suggests a difference between the simulated and experimental surface structures at $T - T_m = -62$ K, potentially due to surface restructuring over timescales much longer than those probed by MD simulations, as indicated by recent AFM measurements.[19] The effects of surface restructuring on the vSFG spectrum of the air/ice interface at low temperatures will be the focus of a forthcoming study.

Interestingly, the intensity of the free-OH peak is predicted to increase by a factor of $\sim$2 when cooling from $T - T_m = -2$ K to $T - T_m = -62$ K in both classical MD and quantum Te-PIGS vSFG spectra. While this trend is not observed in the experimental vSFG spectra reported in Refs. 26 and 27, it aligns with measurements of the orientational order parameter in Ref. 21. Analyses of the underlying molecular configurations reveal that this intensity

increase in the free-OH peak at lower temperatures correlates with a greater number of dangling OH bonds and reduced angular motion (see subsection "Spectra Decomposition" below).

Overall, the vSFG spectra calculated at different temperatures from Te-PIGS simulations effectively reproduce all experimental spectral features except for the emergence of the low-frequency positive peak at $T - T_m \approx -60$ K, without requiring any *ad hoc* frequency shifts.

Role of nuclear quantum effects. While it is common for computational studies to include NQEs in the vibrational spectra of water and ice by applying an *ad hoc* frequency shift to the spectral features calculated from classical MD simulations, different hydrogen-bonding environments give rise to NQEs of varying magnitudes (Fig.2). This suggests that applying a constant red shift across the entire frequency range of the OH-stretch vibrations, as shown in Fig. 2a, is insufficient for accurately modeling the experimental spectrum. Specifically, the air/ice interface comprises three distinct hydrogen-bonding environments: (i) free OH groups (gas-phase-like), (ii) hydrogen-bonded OH groups in the QLL region (liquid-water-like), and (iii) hydrogen-bonded OH groups in bulk ice (ice-like), each of which exhibit different NQEs. Comparison between the classical MD and quantum Te-PIGS vSFG spectra indicates that NQEs induce shifts of varying magnitudes based on the underlying hydrogen-bonding structure, ranging from 160 cm^{-1} for the free OH peak to 187 cm^{-1} for the hydrogen-bonded band.

Spectral decomposition. Classifying each water molecule by the number of hydrogen bonds it donates to (D) or accepts from (A) neighboring molecules provides a useful framework for interpreting the features of the vSFG spectra of aqueous interfaces. The spectral features observed in the vSFG spectrum of the air/ice interface measured in Ref. 27 were assigned to delocalized OH-stretch vibrations through comparisons with IR and Raman spectra of bulk ice. Additionally, in the same study, MD simulations were used to assign the positive

feature at 3550 cm^{-1} to both symmetric OH-stretch vibrations of 2D-1A water molecules (i.e., water molecules donating two hydrogen bonds and accepting one hydrogen bond) and asymmetric OH-stretch vibrations of 2D-2A water molecules (i.e., water molecules donating and accepting two hydrogen bonds).

To gain a molecular-level understanding of the QLL, we dissected the Te-PIGS vSFG spectra shown in Fig. 2 based on molecular monolayers (ML), bilayers (BL), orientations, and hydrogen-bonding topologies. Fig. 3 presents the spectral decomposition of the quantum Te-PIGS vSFG spectra at $T - T_{\mathrm{m}} = -62$ K, -12 K, and -2 K with respect to odd and even molecular layers. At $T - T_{\mathrm{m}} = -62$ K, monolayer 1 (ML1) and monolayer 2 (ML2) exhibit distinct spectral features compared to the other layers. The corresponding spectral decomposition from analogous classical MD simulations are shown in Fig. S12 of the Supporting Information. The free-OH peak at 3700 cm^{-1} originates from molecules in ML1, while the peak at 3550 cm^{-1} arises from molecules in ML2. Molecules in both ML1 and ML2 contribute to the hydrogen-bonded peak at 3300 cm^{-1}. As shown in Fig. S6 of the Supporting Information, the vSFG spectrum of the air/ice interface at $T - T_{\mathrm{m}} = -62$

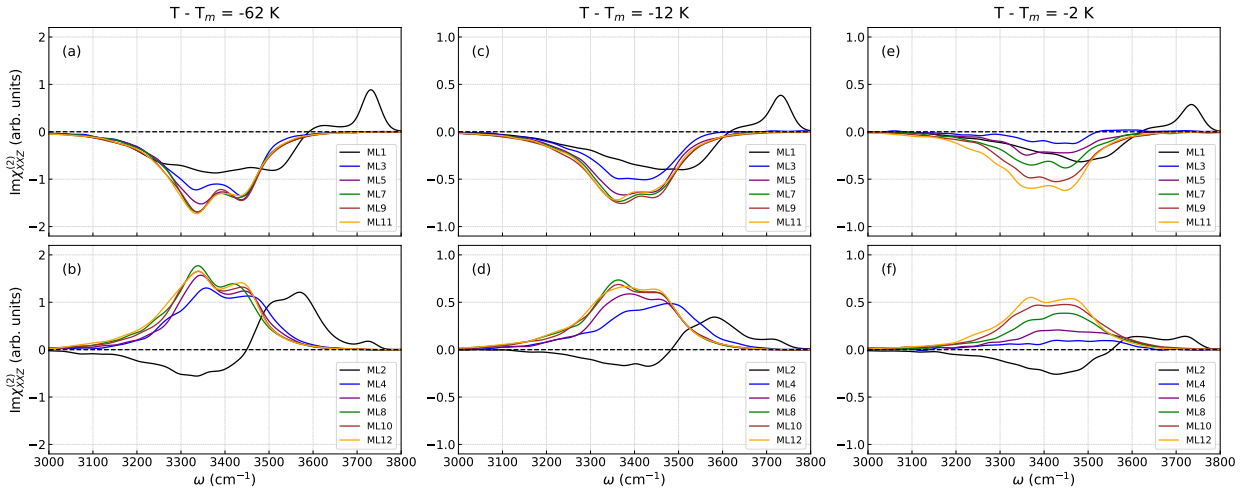

Figure 3: Spectral decomposition of quantum Te-PIGS vSFG spectra at $T - T_m = -62$ K, $T - T_m = -12$ K, and $T - T_m = -2$ K, performed with respect to odd and even monolayers. All vSFG spectra were calculated for the SSP polarization combination. The y-axis ranges differ between the left, middle, and right columns for better clarity.

K is largely due to molecules located in the topmost bilayer (BL1). The contributions from molecules in BL2 result in a small intensity increase of the negative band at 3300 cm^{-1} and the positive peak at 3450 cm^{-1}. Contributions from deeper odd and even layers tend to cancel out as depth increases. At $T - T_m = -12$ K, monolayers ML1 and ML2 remain distinct, while ML3 and ML4 become disordered and contribute to the interfacial region. As the temperature approaches the melting point, at $T - T_m = -2$ K, monolayers ML1 to ML8 display distinct features and become increasingly disordered compared to the bulk layers, leading to a progressively thicker QLL. Previous studies have also reported a decrease in the orientational order parameter of free-OH groups at the air/ice interface at temperatures above 200 K, attributing this to increased surface disorder and the onset of the QLL.[21] Additional analyses are reported in the Supporting Information. Specifically, Fig. S9 illustrates the effect of varying the dipole moment and polarizability cross-correlation cutoff, Fig. S10 highlights the impact of interlayer dipole-polarizability coupling, and Fig. S11 examines the role of many-body electrostatic contributions in calculating the vSFG spectra.

The quantum Te-PIGS vSFG spectrum calculated at $T - T_m = -62$ K is decomposed in Fig. 4a-d based on contributions from molecules located within the two topmost ice bilayers (BL1 and BL2) and in Fig. 4e-h based on the orientations of molecules relative to the ice surface within the four topmost ice monolayers (ML1, ML2, ML3, and ML4). In this analyses, all water molecules are grouped into four categories based on their orientations: (i) 'ML stitching down', (ii) 'BL stitching down', (iii) 'ML stitching up', and (iv) 'BL stitching up' (see Section VII of the Supporting Information for specific details). According to this classification, 'BL stitching up' and 'BL stitching down' refer to water molecules whose OH bonds form hydrogen bonds between two bilayers, whereas 'ML stitching up' and 'ML stitching down' refer to water molecules whose OH bonds form hydrogen bonds between two monolayers. The 'BL stitching up' molecules in ML1 contribute to both the free-OH peak and the negative band at 3300 cm^{-1} while 'BL stitching down' molecules in ML2 contribute to the peaks at 3550 cm^{-1} and 3300 cm^{-1}. The 'ML stitching down' molecules

in ML1 contribute to the negative peak at 3550 cm^{-1} while the 'ML stitching up' molecules in ML2 contribute to the positive peak at 3300 cm^{-1}. In ML1, the OH bonds in 'ML stitching down' molecules vibrate at a different frequency compared to the OH bonds in 'ML stitching up' molecules in ML2. However, 'ML stitching down' configurations in ML3 and 'ML stitching up' configurations in ML4 both vibrate at 3300 cm^{-1}, resulting in their contributions canceling each other out. Fig. S13 in the Supporting Information shows that 'BL stitching down' molecules and 'BL stitching up' molecules in BL2 do not cancel out each other's contributions completely, resulting in an overall positive peak at 3450 cm^{-1} and a simultaneous increase in the intensity of the negative peak at 3300 cm^{-1}. This suggests that, for the intensity of the 3300 cm^{-1} peak to match the experimental spectrum, either

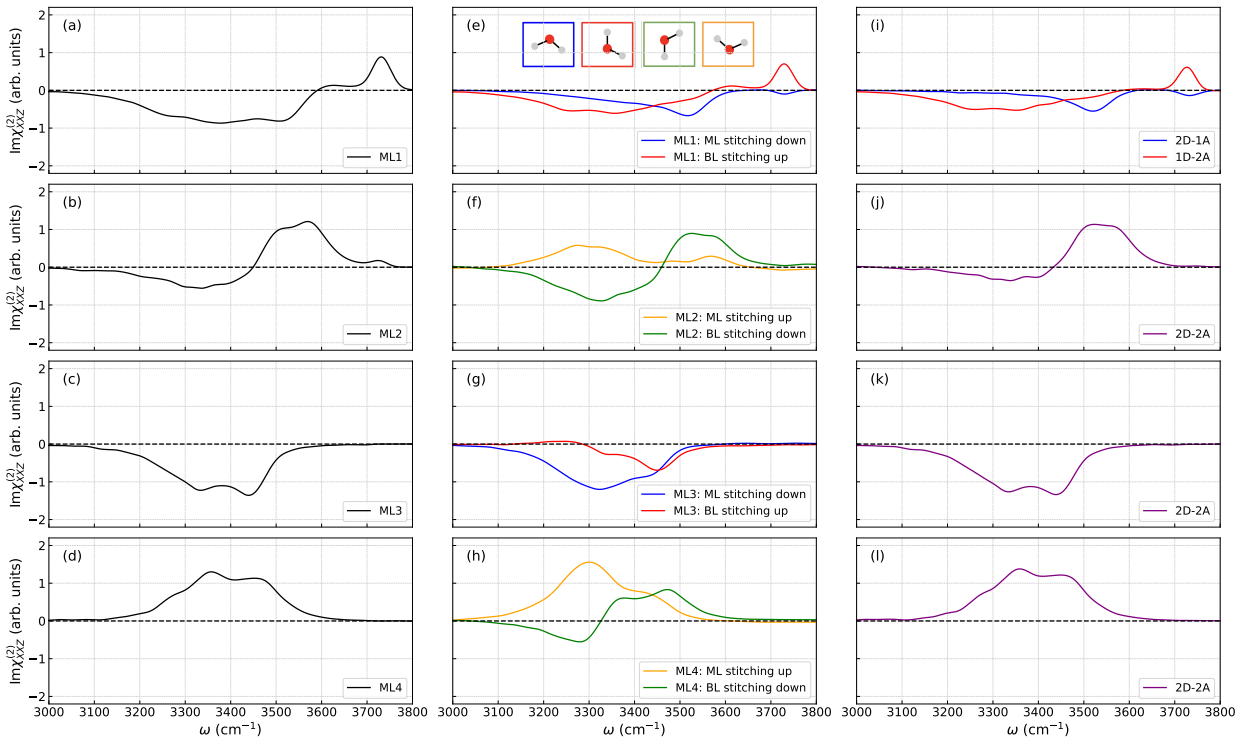

Figure 4: Spectral decomposition of the quantum Te-PIGS vSFG spectrum at $T - T_m = -62$ K, performed with respect to odd and even monolayers (left column), molecular orientations (middle column), and hydrogen-bonding topologies in ML1, ML2, ML3, and ML4 (right column). Inset shows the four possible molecular orientations (panel e). The three hydrogen-bonding topologies are shown in Fig. S19 of the Supporting Information. All vSFG spectra were calculated for the SSP polarization combination.

the number of 'BL stitching up' molecules must be significantly lower than that of 'BL stitching down' molecules, or the 'BL stitching up' molecules must vibrate at a different frequency than their 'BL stitching down' counterparts. The apparent discrepancy between the experimental and simulated vSFG spectra found in Fig. 2 indicates a structural difference between the experimental and simulated ice surfaces at $T - T_{\mathrm{m}} = -62$ K, possibly due to surface restructuring occurring over time scales longer than those probed by MD simulations.

Fig. 4i-l show the spectral decomposition of the quantum Te-PIGS vSFG spectrum calculated at $T - T_m = -62$ K based on hydrogen-bonding topologies of water molecules located in the ML1, ML2, ML3, and ML4 monolayers. In ML1, 'bilayer stitching up' molecules correspond to 1D-2A hydrogen-bonding topologies, which contribute to the free-OH peak, while 'monolayer stitching down' molecules correspond to 2D-1A hydrogen-bonding topologies, contributing to the 3550 cm^{-1} peak. In contrast, molecules located in the ML2, ML3, and ML4 layers are primarily composed of fully-coordinated 2D-2A molecules, with contributions from molecules in ML3 and ML4 effectively canceling each other out (Fig. 4k-l). Figs. S14-S18 of the Supporting Information show similar spectral decomposition for both classical MD and quantum Te-PIGS vSFG spectra calculated at $T - T_m = -12$ K and $T - T_m = -2$ K.

Importantly, Fig. 4 shows that the free-OH peak arises primarily from the vertical OH bonds of the 'BL stitching up' molecules in ML1. The angular distribution of these vertical OH bonds at $T - T_m = -62$ K shows a higher probability density than at $T - T_m = -12$ K and $T - T_m = -2$ K (see Figs. S7 and S8 of the Supporting Information). This indicates a greater number of dangling OH bonds at lower temperatures, with reduced angular motion, which explains the twofold increase in free-OH peak intensity observed in both classical MD and quantum Te-PIGS vSFG spectra as the temperature decreases (Fig. 2).

Comparison with the air/water interface. Fig. 5 shows the quantum Te-PIGS vSFG spectra calculated with MB-pol(2023) for the air/water interface at 298 K and the air/ice

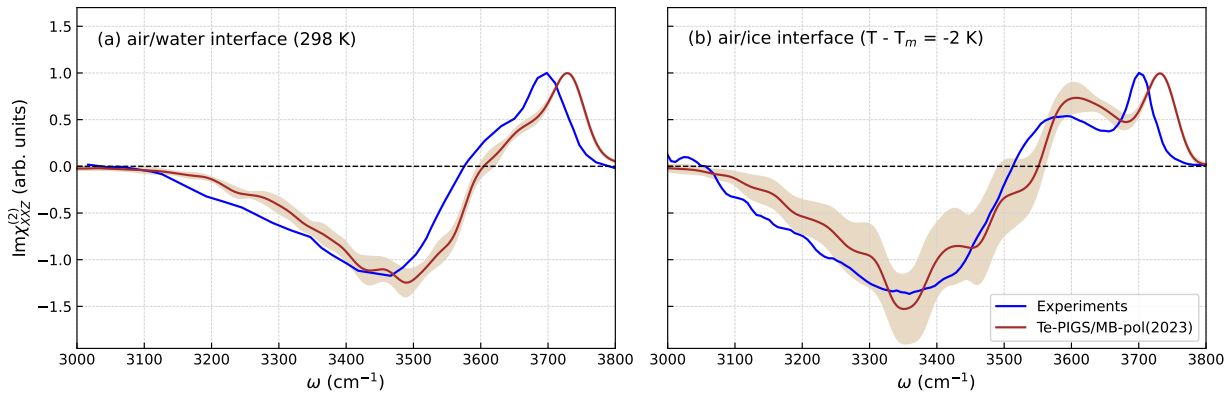

Figure 5: Quantum Te-PIGS vSFG spectra of the air/water interface at 298 K and air/ice interface at $T - T_m = -2$ K with MB-pol(2023), compared with corresponding experimental spectra.[26,49] All vSFG spectra were calculated for the SSP polarization combination. Error bars on the simulated vSFG spectra represent 95% confidence intervals, calculated from the standard error of the mean across 10 and 20 independent trajectories for the air/water and air/ice interfaces, respectively.

interface at $T - T_m = -2$ K, along with the corresponding experimental data. While the vSFG spectra of both interfaces display a pronounced peak at ∼3700 cm^{-1}, corresponding to dangling OH bonds exposed to air, the air/ice interface spectrum features a distinct positive peak at ∼3550 cm^{-1} and a broader, more intense negative band between 3100 and 3500 cm^{-1}, resulting from the stretching vibrations of hydrogen-bonded OH groups. This band is red-shifted by approximately 100 cm^{-1} compared to the air/water interface, reflecting the stronger hydrogen bonds in ice. For both interfaces, quantum Te-PIGS simulations with MB-pol(2023) predict vSFG spectra in close quantitative agreement with experimental data, with deviations consistently within $\Delta\omega \leq 30$ cm^{-1} for all spectral features, achieved without the use of any *ad hoc* frequency shifts. These results further demonstrate the realism of the MB-pol(2023) potential and underscore the importance of NQEs.

Conclusion

In this study, we leveraged state-of-the-art quantum dynamics simulations with the highly accurate MB-pol(2023) many-body potential to provide new insights into the air/ice inter-

face. By dissecting the vSFG spectrum at the molecular level, we revealed distinct spectral features arising from individual monolayers of ice, identifying local hydrogen-bonding environments that govern the formation of the QLL at the interface.

Our simulations show that the QLL begins to form with the melting of approximately one bilayer at temperatures ∼60 K below the melting point. This process is characterized by distinct shifts in the OH stretching frequencies of 'BL stitching up' and 'ML stitching down' water molecules within the two topmost monolayers, highlighting subtle changes in the underlying hydrogen-bonding network. Furthermore, we demonstrated that simple red-shifting applied to vSFG spectra calculated from classical MD simulations is insufficient for accurately capturing NQEs, underscoring the necessity of fully quantum-mechanical approaches for modeling ice surfaces. Importantly, our analyses suggest that surface restructuring may occur at lower temperatures and be responsible for the appearance of specific features in the vSFG spectra. These insights suggest that surface defects, which may vary depending on how the air/ice interface is prepared, can play a critical role in shaping the properties of the QLL at different temperatures, introducing new complexity to its molecular structure.

This study advances our understanding of the QLL, offering a molecular-level picture that has eluded previous studies. Our results are in agreement with the experimental data and provide a new baseline for exploring how the structure of the ice surface influences chemical and physical processes of relevance to a variety of fields, including atmospheric chemistry, cryopreservation, and the development of novel materials. The realism of our MB-pol simulations sets a new benchmark for future studies of water and ice interfaces, further highlighting the importance of many-body interactions and nuclear quantum effects in accurately predicting the behavior of water across different phases.

Methods

A schematic overview of the methodology employed to equilibrate the air/ice interface and calculate the corresponding vSFG spectra and spectral decomposition is shown in Fig. S1 of the Supporting Information.

Molecular dynamics simulations. All the equilibration simulations were performed using DeePMD[50] combined with LAMMPS.[51] The classical vSFG spectra were calculated from classical MD simulations in the NVE ensemble performed using MBX[52] combined with LAMMPS.[51] The quantum vSFG spectra were calculated from Te-PIGS simulations performed using MBX[52] combined with DeePMD[50] and i-PI.[53] The initial proton disordered configuration of bulk ice I_h was prepared using GenIce,[54] following the Bernal-Fowler ice rules.[55] All simulations were carried out in periodic boundary conditions for an ice slab containing $N = 1296$ water molecules. The following potentials were used in the simulations: (a) DNN@MB-pol for equilibration, (b) MB-pol(2023) for classical MD simulations in the NVE ensemble and PIMD simulations in the NVT ensemble, (c) MB-pol(2023) + the QC@MB-pol(2023) quantum correction potential for the Te-PIGS simulations in the NVE ensemble. Specific details about the training and validation of the quantum correction QC@MB-pol(2023) potential and Te-PIGS simulations are discussed in the Supporting Information.

vSFG spectrum calculations. The many-body dipole moment surface (MB-μ) and polarizability surface (MB-α) were used to compute the dipole moments and polarizability tensors. The MB-μ and MB-α models were introduced in Ref. 43 based on a detailed analysis of the convergence of the many-body expansion of the total dipole moment and polarizability of water.[56] Comparisons with other models show that MB-μ quantitatively captures many-body effects in representing the total dipole moment of liquid water, enabling accurate predictions of all features in its infrared spectrum.[57] In addition, MB-μ and MB-α were also shown to accurately reproduce the lineshapes of infrared and Raman spectra of liquid water at different temperatures[46] and various ice phases,[47,48] as well as the vSFG spectra of the

air/water interface at different temperatures.[44,45] The second-order susceptibility $\chi^{(2)}_{ijk}(\omega)$ was calculated from the Fourier transform of the time correlation function (TCF) of the dipole moment and polarizability tensor.[58,59] The total time correlation function was computed as a sum of the autocorrelation function and truncated cross-correlation function over all water molecules within a cutoff distance of 4.0 Å.[44,45] Further details of the vSFG spectra and spectral decomposition calculations are discussed in the Supporting Information.

Acknowledgement

We thank Mary Jane Shultz for several insightful discussions and Venkat Kapil for his help with setting up the Te-PIGS simulations. This research was supported by the Air Force Office of Scientific Research under award FA9550-20-1-0351. Computational resources were provided by the Department of Defense High Performance Computing Modernization Program (HPCMP) and the Scientific Computing Core at the Flatiron Institute, a division of the Simons Foundation.

Supporting Information Available

The Supporting Information is available free of charge and includes the following details: initial ice configuration, potential energy surfaces, the Te-PIGS method, equilibration and production runs, vSFG spectra and spectral decomposition calculations, a schematic representation of the methodology, the distribution of the environment similarity kernel, the density profile and number of melted bilayers, and additional analyses of the vSFG spectral decomposition.

References

(1) Petrenko, V. F.; Whitworth, R. W. *Physics of Ice*; Oxford University Press, Oxford, 1999.

(2) Dash, J.; Rempel, A.; Wettlaufer, J. The Physics of Premelted Ice and its Geophysical Consequences. *Rev. Mod. Phys.* **2006**, *78*, 695–741.

(3) Salzmann, C. G. Advances in the Experimental Exploration of Water's Phase Diagram. *J. Chem. Phys.* **2019**, *150*, 060901.

(4) Sosso, G. C.; Chen, J.; Cox, S. J.; Fitzner, M.; Pedevilla, P.; Zen, A.; Michaelides, A. Crystal Nucleation in Liquids: Open Questions and Future Challenges in Molecular Dynamics Simulations. *Chem. Rev.* **2016**, *116*, 7078–7116.

(5) Shultz, M. J. Crystal Growth in Ice and Snow. *Phys. Today* **2018**, *71*, 34–39.

(6) Abbatt, J. P. Interactions of Atmospheric Trace Gases with Ice Surfaces: Adsorption and Reaction. *Chem. Rev.* **2003**, *103*, 4783–4800.

(7) Sun, Z.; Pan, D.; Xu, L.; Wang, E. Role of Proton Ordering in Adsorption Preference of Polar Molecule on Ice Surface. *Proc. Natl. Acad. Sci. U.S.A.* **2012**, *109*, 13177–13181.

(8) Faraday, M. On Certain Conditions of Freezing Water. *Journal of the Franklin Institute, of the State of Pennsylvania, for the Promotion of the Mechanic Arts; Devoted to Mechanical and Physical Science, Civil Engineering, the Arts and Manufactures, and the Recording of American and Other Patent Inventions (1828-1851)* **1850**, *20*, 283.

(9) Rosenberg, R. Why Is Ice Slippery? *Phys. Today* **2005**, *58*, 50–54.

(10) Sazaki, G.; Zepeda, S.; Nakatsubo, S.; Yokomine, M.; Furukawa, Y. Quasi-Liquid Layers on Ice Crystal Surfaces Are Made up of Two Different Phases. *Proc. Natl. Acad. Sci. U.S.A.* **2012**, *109*, 1052–1055.

(11) Asakawa, H.; Sazaki, G.; Nagashima, K.; Nakatsubo, S.; Furukawa, Y. Two Types of Quasi-liquid Layers on Ice Crystals Are Formed Kinetically. *Proc. Natl. Acad. Sci. U.S.A.* **2016**, *113*, 1749–1753.

(12) Murata, K.-i.; Asakawa, H.; Nagashima, K.; Furukawa, Y.; Sazaki, G. Thermodynamic Origin of Surface Melting on Ice Crystals. *Proc. Natl. Acad. Sci. U.S.A.* **2016**, *113*, E6741–E6748.

(13) Furukawa, Y.; Yamamoto, M.; Kuroda, T. Ellipsometric Study of the Transition Layer on the Surface of an Ice Crystal. *J. Cryst. Growth* **1987**, *82*, 665–677.

(14) Dosch, H.; Lied, A.; Bilgram, J. Glancing-Angle X-ray Scattering Studies of the Premelting of Ice Surfaces. *Surf. Sci.* **1995**, *327*, 145–164.

(15) Bluhm, H.; Ogletree, D. F.; Fadley, C. S.; Hussain, Z.; Salmeron, M. The Premelting of Ice Studied with Photoelectron Spectroscopy. *J. Phys. Condens. Matter* **2002**, *14*, L227.

(16) Döppenschmidt, A.; Butt, H.-J. Measuring the Thickness of the Liquid-like Layer on Ice Surfaces with Atomic Force Microscopy. *Langmuir* **2000**, *16*, 6709–6714.

(17) Morgenstern, M.; Müller, J.; Michely, T.; Comsa, G. The Ice Bilayer on Pt(111): Nucleation, Structure and Melting. *Z. Phys. Chem.* **1997**, *198*, 43–72.

(18) Slater, B.; Michaelides, A. Surface Premelting of Water Ice. *Nat. Rev. Chem.* **2019**, *3*, 172–188.

(19) Hong, J.; Tian, Y.; Liang, T.; Liu, X.; Song, Y.; Guan, D.; Yan, Z.; Guo, J.; Tang, B.; Cao, D.; Guo, J.; Chen, J.; Pan, D.; Xu, L.-M.; Wang, E.-G.; Jiang, Y. Imaging Surface Structure and Premelting of Ice Ih with Atomic Resolution. *Nature* **2024**, *630*, 375–380.

(20) Shen, Y. R.; Ostroverkhov, V. Sum-Frequency Vibrational Spectroscopy on Water Interfaces: Polar Orientation of Water Molecules at Interfaces. *Chem. Rev.* **2006**, *106*, 1140–1154.

(21) Wei, X.; Miranda, P. B.; Shen, Y. Surface Vibrational Spectroscopic Study of Surface Melting of Ice. *Phys. Rev. Lett.* **2001**, *86*, 1554.

(22) Wei, X.; Miranda, P. B.; Zhang, C.; Shen, Y. Sum-Frequency Spectroscopic Studies of Ice Interfaces. *Phys. Rev. B* **2002**, *66*, 085401.

(23) Groenzin, H.; Li, I.; Buch, V.; Shultz, M. J. The Single-Crystal, Basal Face of Ice I_h Investigated with Sum Frequency Generation. *J. Chem. Phys.* **2007**, *127*, 214502.

(24) Shultz, M. J.; Bisson, P.; Groenzin, H.; Li, I. Multiplexed Polarization Spectroscopy: Measuring Surface Hyperpolarizability Orientation. *J. Chem. Phys.* **2010**, *133*, 054702.

(25) Li Barnett, I.; Groenzin, H.; Shultz, M. J. Hydrogen Bonding in the Hexagonal Ice Surface. *J. Phys. Chem. A* **2011**, *115*, 6039–6045.

(26) Smit, W. J.; Bakker, H. J. The Surface of Ice Is Like Supercooled Liquid Water. *Angew. Chem. Int. Ed.* **2017**, *56*, 15540–15544.

(27) Smit, W. J.; Tang, F.; Nagata, Y.; Sánchez, M. A.; Hasegawa, T.; Backus, E. H.; Bonn, M.; Bakker, H. J. Observation and Identification of a New OH Stretch Vibrational Band at the Surface of Ice. *J. Phys. Chem. Lett.* **2017**, *8*, 3656.

(28) Nojima, Y.; Suzuki, Y.; Takahashi, M.; Yamaguchi, S. Proton Order Toward the Surface of Ice I_h Revealed by Heterodyne-detected Sum Frequency Generation Spectroscopy. *J. Phys. Chem. Lett* **2017**, *8*, 5031.

(29) Sánchez, M. A.; Kling, T.; Ishiyama, T.; van Zadel, M.-J.; Bisson, P. J.; Mezger, M.; Jochum, M. N.; Cyran, J. D.; Smit, W. J.; Bakker, H. J.; Shultz, M. J.; Morita, A.; Donadio, D.; Nagata, Y.; Bonn, M.; Backus, E. H. G. Experimental and Theoretical

Evidence for Bilayer-by-bilayer Surface Melting of Crystalline Ice. *Proc. Natl. Acad. Sci. U.S.A.* **2017**, *114*, 227–232.

(30) Buch, V.; Tarbuck, T.; Richmond, G.; Groenzin, H.; Li, I.; Shultz, M. Sum Frequency Generation Surface Spectra of Ice, Water, and Acid Solution Investigated by an Exciton Model. *J. Chem. Phys.* **2007**, *127*, 204710.

(31) Buch, V.; Groenzin, H.; Li, I.; Shultz, M.; Tosatti, E. Proton Order in the Ice Crystal Surface. *Proc. Natl. Acad. Sci. U.S.A.* **2008**, *105*, 5969–5974.

(32) Ishiyama, T.; Takahashi, H.; Morita, A. Origin of Vibrational Spectroscopic Response at Ice Surface. *J. Phys. Chem. Lett.* **2012**, *3*, 3001.

(33) Wan, Q.; Galli, G. First-Principles Framework to Compute Sum-Frequency Generation Vibrational Spectra of Semiconductors and Insulators. *Phys. Rev. Lett.* **2015**, *115*, 246404.

(34) Bore, S. L.; Paesani, F. Realistic Phase Diagram of Water from "First Principles" Data-driven Quantum Simulations. *Nat. Commun.* **2023**, *14*, 3349.

(35) Zhai, Y.; Caruso, A.; Bore, S. L.; Luo, Z.; Paesani, F. A "Short Blanket" Dilemma for a State-of-the-Art Neural Network Potential for Water: Reproducing Experimental Properties or the Physics of the Underlying Many-Body Interactions? *J. Chem. Phys.* **2023**, *158*, 084111.

(36) Zhai, Y.; Rashmi, R.; Palos, E.; Paesani, F. Many-Body Interactions and Deep Neural Network Potentials for Water. *J. Chem. Phys.* **2024**, *160*, 144501.

(37) Reddy, S. K.; Straight, S. C.; Bajaj, P.; Huy Pham, C.; Riera, M.; Moberg, D. R.; Morales, M. A.; Knight, C.; Götz, A. W.; Paesani, F. On the Accuracy of the MB-pol Many-Body Potential for Water: Interaction Energies, Vibrational Frequencies, and

Classical Thermodynamic and Dynamical Properties from Clusters to Liquid Water and Ice. *J. Chem. Phys.* **2016**, *145*, 194504.

(38) Palos, E.; Bull-Vulpe, E. F.; Zhu, X.; Agnew, H.; Gupta, S.; Paesani, F. Current Status of the MB-pol Data-Driven Many-Body Potential for Predictive Simulations of Water Across Different Phases. *J. Chem. Theory Comput.* **2024**, *20*, 9269–9289.

(39) Musil, F.; Zaporozhets, I.; Noé, F.; Clementi, C.; Kapil, V. Quantum Dynamics Using Path Integral Coarse-Graining. *J. Chem. Phys.* **2022**, *157*, 181102.

(40) Kapil, V.; Kovács, D. P.; Csányi, G.; Michaelides, A. First-Principles Spectroscopy of Aqueous Interfaces Using Machine-learned Electronic and Quantum Nuclear Effects. *Faraday Discuss.* **2024**, *249*, 50–68.

(41) Zhu, X.; Riera, M.; Bull-Vulpe, E. F.; Paesani, F. MB-pol(2023): Sub-Chemical Accuracy for Water Simulations from the Gas to the Liquid Phase. *J. Chem. Theory Comput.* **2023**, *19*, 3551–3566.

(42) Piaggi, P. M.; Parrinello, M. Calculation of Phase Diagrams in the Multithermal-Multibaric Ensemble. *J. Chem. Phys.* **2019**, *150*, 244119.

(43) Medders, G. R.; Paesani, F. Infrared and Raman Spectroscopy of Liquid Water Through "First-Principles" Many-Body Molecular Dynamics. *J. Chem. Theory Comput.* **2015**, *11*, 1145–1154.

(44) Medders, G. R.; Paesani, F. Dissecting the Molecular Structure of the Air/Water Interface from Quantum Simulations of the Sum-Frequency Generation Spectrum. *J. Am. Chem. Soc.* **2016**, *138*, 3912–3919.

(45) Moberg, D. R.; Straight, S. C.; Paesani, F. Temperature Dependence of the Air/Water Interface Revealed by Polarization Sensitive Sum-Frequency Generation Spectroscopy. *J. Phys. Chem. B* **2018**, *122*, 4356–4365.

(46) Reddy, S. K.; Moberg, D. R.; Straight, S. C.; Paesani, F. Temperature-Dependent Vibrational Spectra and Structure of Liquid Water from Classical and Quantum Simulations With the MB-pol Potential Energy Function. *J. Chem. Phys.* **2017**, *147*, 244504.

(47) Moberg, D. R.; Straight, S. C.; Knight, C.; Paesani, F. Molecular Origin of the Vibrational Structure of Ice I_h. *J. Phys. Chem. Lett.* **2017**, *8*, 2579–2583.

(48) Moberg, D. R.; Sharp, P. J.; Paesani, F. Molecular-Level Interpretation of Vibrational Spectra of Ordered Ice Phases. *J. Phys. Chem. B* **2018**, *122*, 10572–10581.

(49) Nihonyanagi, S.; Kusaka, R.; Inoue, K.-i.; Adhikari, A.; Yamaguchi, S.; Tahara, T. Accurate Determination of Complex $\chi(2)$ Spectrum of the Air/Water Interface. *J. Chem. Phys.* **2015**, *143*, 124707.

(50) Wang, H.; Zhang, L.; Han, J.; Weinan, E. DeePMD-kit: A Deep Learning Package for Many-Body Potential Energy Representation and Molecular Dynamics. *Comput. Phys. Commun.* **2018**, *228*, 178–184.

(51) Thompson, A. P.; Aktulga, H. M.; Berger, R.; Bolintineanu, D. S.; Brown, W. M.; Crozier, P. S.; in 't Veld, P. J.; Kohlmeyer, A.; Moore, S. G.; Nguyen, T. D.; Shan, R.; Stevens, M. J.; Tranchida, J.; Trott, C.; Plimpton, S. J. LAMMPS – A Flexible Simulation Tool for Particle-Based Materials Modeling at the Atomic, Meso, and Continuum Scales. *Comput. Phys. Commun.* **2022**, *271*, 108171.

(52) Riera, M.; Knight, C.; Bull-Vulpe, E. F.; Zhu, X.; Agnew, H.; Smith, D. G. A.; Simmonett, A. C.; Paesani, F. MBX: A Many-Body Energy and Force Calculator for Data-Driven Many-Body Simulations. *J. Chem. Phys.* **2023**, *159*, 054802.

(53) Kapil, V.; Rossi, M.; Marsalek, O.; Petraglia, R.; Litman, Y.; Spura, T.; Cheng, B.; Cuzzocrea, A.; Meißner, R. H.; Wilkins, D. M.; Juda, P.; Bienvenue, S. P.; Fang, W.; Kessler, J.; Poltavsky, I.; Vandenbrande, S.; Wieme, J.; Corminboeuf, C.; Kühne, T. D.;

Manolopoulos, D. E.; Markland, T. E.; Richardson, J. O.; Tkatchenko, A.; Tribello, G. A.; Van Speybroeck, V.; Ceriotti, M. i-PI 2.0: A Universal Force Engine for Advanced Molecular Simulations. *Comput. Phys. Commun.* **2019**, *236*, 214–223.

(54) Matsumoto, M.; Yagasaki, T.; Tanaka, H. GenIce: Hydrogen-Disordered Ice Generator. *J. Comp. Chem.* **2018**, *39*, 61–64.

(55) Bernal, J. D.; Fowler, R. H. A Theory of Water and Ionic Solution, with Particular Reference to Hydrogen and Hydroxyl Ions. *J. Chem. Phys.* **1933**, *1*, 515.

(56) Medders, G. R.; Paesani, F. Many-Body Convergence of the Electrostatic Properties of Water. *J. Chem. Theory Comput.* **2013**, *9*, 4844–4852.

(57) Medders, G. R.; Paesani, F. On the Interplay of the Potential Energy and Dipole Moment Surfaces in Controlling the Infrared Activity of Liquid Water. *J. Chem. Phys.* **2015**, *142*, 104102.

(58) Morita, A.; Hynes, J. T. A Theoretical Analysis of the Sum Frequency Generation Spectrum of the Water Surface. II. Time-Dependent Approach. *J. Phys. Chem. B* **2002**, *106*, 673–685.

(59) Nagata, Y.; Mukamel, S. Vibrational Sum-Frequency Generation Spectroscopy at the Water/Lipid Interface: Molecular Dynamics Simulation Study. *J. Am. Chem. Soc.* **2010**, *132*, 6434–6442.

TOC Graphic